Engineering Structures 306 (2024) 117858

Contents lists available at ScienceDirect

Engineering Structures

journal homepage: www.elsevier.com/locate/engstruct

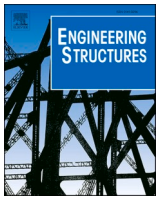

Investigations on the fatigue loading of thin-walled and resource-efficient UHPFRC segmental bridges

Marvin Wilkening *, Linus Joachim, Vincent Oettel

Institute of Concrete Construction, Leibniz University Hannover, Appelstraße 9a, 30167 Hannover, Germany

ARTICLE INFO

Keywords:
UHPFRC
Segmental Bridges
Numerical Investigations
FEM
Fatigue loading
Resource efficiency
Sustainability

ABSTRACT

Many reinforced concrete and prestressed concrete bridges are defective or can no longer withstand the increased traffic loads for a sufficiently long time. In the long term, they will have to be replaced by new structures. In previous reinforced concrete and prestressed concrete bridges, fatigue loading (e.g. traffic, wind) is rarely a problem with regard to the concrete, especially since the cyclic traffic loads are relatively low compared to the static dead loads due to a solid construction method. However, for reasons of sustainability and compliance with climate targets, future structures and bridges should be built in a resource-efficient and materials-compatible manner, while at the same time fast and durable. A target-oriented approach to this is segmental bridge construction with keyed dry joints made of ultra-high-performance fiber-reinforced concrete (UHPFRC). In these bridge structures the fatigue loads could become more relevant due to the slenderness of the thin-walled UHPFRC bridges superstructure and fatigue problems could occur. In order to investigate this in more detail, FE investigations on segmental box girder bridges under variation of the concrete strength (NSC, HSC and UHPFRC) were carried out, while optimising the cross-section dimensions. It was shown that due to the performance of UHPFRC and the associated cross-section optimisation, an exponential increase in the ratio of cyclic live loads to static dead loads and thus an exponential increase in fatigue loading occurs at thin-walled and resource-efficient UHPFRC segmental bridges compared to NSC and HSC bridges and that this can become relevant for the design of such bridges.

1. Introduction

A large number of reinforced concrete and prestressed concrete bridges for example in Germany, USA and Canada. [1–3] are defective or can no longer withstand the increased traffic loads for a sufficiently long time. They will have to be replaced in the long term. Fig. 1 shows the distribution of built bridge with respect to their area of a major German city by year of construction and proportional forecast of replacement construction after 80 years from [1]. It can be seen that the majority of bridges were built between 1950 and 1980. This is due to the need for new infrastructure after the Second World War, which destroyed many bridges in Germany. Although the bridges built were actually designed for a service life of 100 years, there are already very clear deficiencies in terms of load-bearing capacity and durability. On the one hand, this is due to the building materials, construction methods and design approaches used at the time and on the other hand, the increased traffic loads already mentioned contribute to the continuous damage process [4].

Conventional bridge construction using in-situ concrete is, on the one hand, very susceptible to defects and dependent on the weather, so that the quality of execution declines and the durability and service life of the bridge is reduced. On the other hand, this construction method represents an immense intervention in road traffic, which is associated with traffic jams, long detours and very high CO_2 emissions as well as

Abbreviations: f_{cd}, Design value of concrete compressive strength; $f_{cd,fat}$, Design value of concrete compressive fatigue strength; $f_{ctd,fat}$, Design value of concrete tensile fatigue strength; $f_{ctk;0,05}$, Characteristic axial tensile strength of concrete; f_{ctm}, Mean value of axial tensile strength of concrete; f_{ck}, Characteristic compressive cylinder strength of concrete at 28 days; H, Hight of the bridges cross-section; b_w, Thickness of the bridge cross-section web; α_{cc}, Coefficient taking account of long term effects; $\beta_{cc}t_0$, Coefficient for concrete strength at first load application; γ_c, Partial factor for concrete; $\gamma_{c,fat}$, Partial factor for fatigue of concrete; $\Delta\sigma_c$, Compressive stress range; $\Delta\tau_c$, Shear stress range; σ_c, Compressive stress in the concrete; $\sigma_{c,max}$, Maximum compressive stress; $\sigma_{c,min}$, Minimum compressive stress; $\tau_{c,max}$, Maximum shear stress; $\tau_{c,min}$, Minimum shear stress.

* Corresponding author.
E-mail address: wilkening@ifma.uni-hannover.de (M. Wilkening).

https://doi.org/10.1016/j.engstruct.2024.117858
Received 1 December 2023; Received in revised form 6 February 2024; Accepted 10 March 2024
Available online 20 March 2024

very high economic damage. Segmental bridge construction with keyed dry joints made of ultra-high-performance fiber-reinforced concrete (UHPFRC) is an extremely effective, forward-looking, economical, ecological and thus sustainable alternative (e.g. [1,5–9]) as the combination of the high performance of UHPFRC (e.g. [10–13]) and the segmental construction method allows very thin-walled, slender and material-optimized bridge structures to be built in a short time (e.g. [14–18]). In addition to static loads, bridge structures are also subject to high cyclic loads, mainly from traffic (and wind). It must be taken into account that slender and filigree structures are more susceptible to fatigue loading. In the case of thin-walled UHPFRC bridges, the lower dead loads result in a larger ratio between cyclic (live) and static (dead and construction) loads compared to more compact bridges made of normal strength concrete, which can lead to less favorable fatigue loading. In this context, the compressive stresses in the concrete with regard to the thin-walled cross-sections and the shear stresses with regard to the segmental joints are of decisive interest. In addition, load changes of $> 2 \bullet 10^8$ occur, partly as a result of the high cyclic loading and the service life (service life of UHPFRC $>$ 100 years), which cannot be neglected and may possibly lead to fatigue problems in thin-walled UHPFRC structures. However, it must also be taken into account that, according to relevant guidelines, the joints must be completely under compressive stresses under service load levels, so that only a small fatigue stress may result.

If segmental concrete towers of hybrid wind turbines are considered here, which are made of circular precast segments with smooth dry joints and external prestressing (e.g. [19–23]), DIN 18088–2 [24] requires, among other things, a fatigue design of the concrete under compression or shear loading. Due to the smooth dry joints, an increase in stresses of 15% or 35% compared to monolithic concrete towers with continuous reinforcement must be provided for in the fatigue design, although the smooth dry joints are fully subjected to compressive stress. One of the reasons for this is that the joints represent discontinuity areas where an undisturbed area cannot be assumed. However, it should also be mentioned at this point that the increase in stress in smooth dry joints is a pragmatic assumption that has yet to be experimentally verified.

In order to investigate and quantify the fatigue loading of segmental bridges in more detail, FE investigations were carried out on segmental bridges with box girder cross sections under variation of the concrete strength (NSC, HSC and UHPFRC) and the cross section dimensions were optimized in the course of the design (= thin-walled and material-optimized cross sections). Subsequently, the resulting maximum and minimum stresses as well as the stress range of the compressive and shear stresses at the relevant locations were evaluated and analyzed for the individual variants. In the course of the investigations, it became clear that the high strength and durability of UHPFRC and an optimised (thin-walled) construction method can take an important step towards more sustainable and resource-efficient bridge construction. The reduction in cross-section and material means that the proportion of dead weight is significantly reduced and the influence of traffic loads increases considerably. This in turn can lead to an increase in fatigue stress for the bridges, as demonstrated by the following investigations.

2. State of research

2.1. UHPFRC segmental bridges

UHPFRC segmental bridge construction is not yet widespread. However, more and more pilot projects are available that demonstrate the advantages of this construction method. An impressive example of a UHPFRC segmental bridge is the pilot bridge PS34 near Grenoble in France (Fig. 2). By combining UHPFRC with the segmental construction method, it was possible to save 120 m^3 of concrete and two supporting piers compared to the conventional in-situ concrete construction method made of C35/45, to shorten the construction time by two months and to complete the erection in winter largely without influencing highway traffic using a truck-mounted crane (low dead weight) [14].

Other UHPFRC segmental bridges constructed worldwide with similar environmental and economic benefits can be found, for example, in [9,10].

2.2. Fatigue loading of UHPFRC bridges

2.2.1. Flexible modular high-speed railway bridge made of UHPFRC

In [25], the development of a flexible modular high-speed railway bridge made of precast UHPFRC segments for the Austrian Railways (OBB) is reported. The aim of the investigations was to be able to temporarily bridge railroad construction sites with more flexible spans (up to max. 28 m) and lower overall heights. The U-shaped precast UHPFRC segments will be connected at the construction site with smooth dry joints and external prestressing to form a bridge superstructure and, due to their low dead weight, directly lifted into place by rail cranes. The superstructure consists of two end segments and *n* filigree standard segments. The end segments are slightly longer and more compact in order to provide sufficient space for the bearing

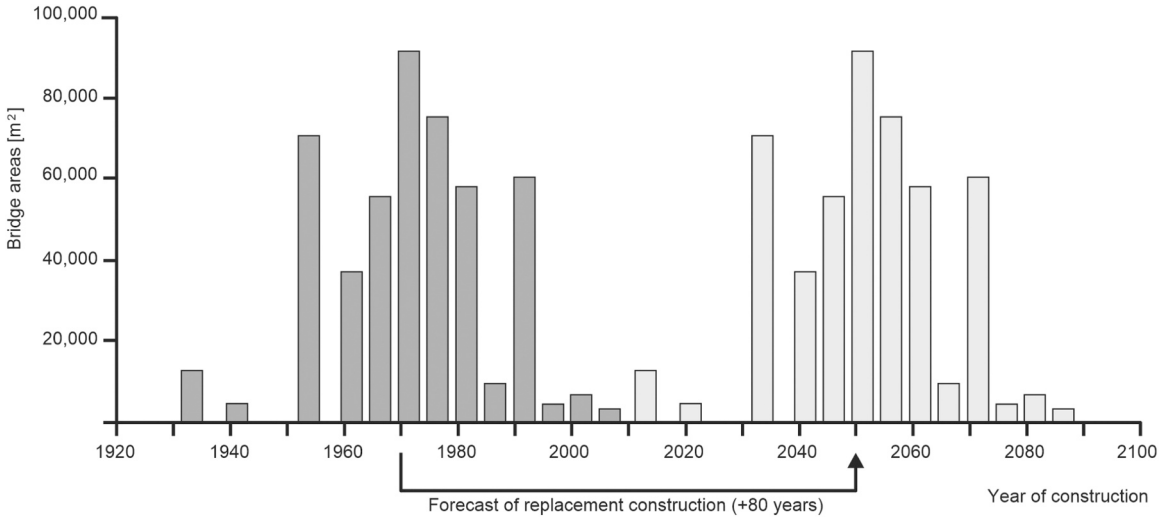

Fig. 1. Distribution of built bridge with respect to their area of a major German city by year of construction and proportional forecast of replacement construction after 80 years (gray bars, right in the diagram) according to [1].

Fig. 2. Bridge PS34: assembly of the 22 UHPFRC segments with 12.0 cm wall thickness and keyed dry joints next to the highway (left) [14], lifting of the 47.7 m long superstructure with only one truck-mounted crane (middle) [15] and finalized bridge (right).
Source: C. Clergue

arrangement, for the expansion joint and for the tendon anchorage. In order to reduce the weight of the standard segments and at the same time save material, the standard segments were designed with thinner trough webs and a hollow base plate, which is provided with a trussed framework in the transverse direction (Fig. 3, left and center). In addition, the (most) external tendons run through the openings of the trussed framework of the base plate (Fig. 3, right). The prestressing was designed so that the dry segment joints are completely under compressive stresses in the serviceability limit state under the rare load combination, and in the ultimate limit state, the gaping of the dry joints is limited to 2/3 of the cross-sectional height. Due to the large web area and a characteristic coefficient of friction of 0.35, the segmental joints are designed without fine profiling with a smooth, CNC-ground surface. The development of the flexible modular bridge made of precast UHPFRC segments was based on extensive FE calculations and experimental tests. In addition, according to [1], a two-year test phase of a prototype will investigate, among other things, how the smooth, CNC-ground UHPFRC segment joints behave under high cyclic loads (fatigue loading resulting from railway operation). Further publications on the findings and results of this test phase are not available in the technical literature.

The fatigue life of the UHPFRC segmental bridge and the individual segments was specified by OBB as 50 years. This led to a massive change in the steel stresses during the fatigue check of the shear reinforcement and ultimately to an amplification of the stirrups by a factor of 1.5. According to [1], this factor or this increase in the shear stresses is due to the increasing influence of the cyclic live loads compared to the lower static dead loads of the lightweight filigree UHPFRC segmental bridge (= larger ratio between cyclic live loads and static dead loads). Further evaluations on the fatigue loading, e.g. on the compressive stresses occurring, are not includes in [1] and [25] or cannot be subsequently analysed on the basis of the information provided.

2.2.2. FE study on segmental bridges made of UHPFRC

Since the load-bearing behavior of segmental bridges made of UHPFRC may differ from that of ordinary segmental bridges made of normal and high strength concrete (NSC and HSC) due to the higher concrete strength and the possible thin cross-sections, the bending load-bearing behavior of segmental bridges with box girder cross-section, external tendons and dry joints under variation of the concrete compressive strength (C55/67, C80/95, C120/145, C180/217) was investigated in [6] using nonlinear finite element calculations. For the design of the segmental bridge, a simplified load model deviating from [26,27] was applied and (only) one load position (maximum bending moment in the center of the span) was investigated. Furthermore, according to [28,29], the concrete compressive stresses were limited to $\sigma_c = 0,45 \bullet f_{ck}$. By varying the concrete compressive strength, the cross-sectional dimensions (web thickness, slab thickness and cross-sectional height) could be significantly reduced, thus increasing the slenderness. The determined cross-sectional dimensions of the segmental bridges C55/67, C80/95, C120/145, C180/217-H18 and C180/217-H24 can be taken from Fig. 4 and Table 1.

This numerical study focuses on the change in compressive stresses at the center of the span and the opening of the segment joints. However, the obtained results can be used for further evaluation on the effects of slenderness of segmental structures on fatigue loading, since the calculated stresses are listed at serviceability level in [6]. Evaluating these results, it can be seen that with increasing concrete grade or more and more slender and thus lighter bridges, the related maximum stresses $\sigma_{c,max}/f_{cd,fat}$ resp. the related minimum stresses $\sigma_{c,min}/f_{cd,fat}$ decrease and the related stress ranges $\Delta\sigma_c/f_{cd,fat}$ remain approximately constant (with

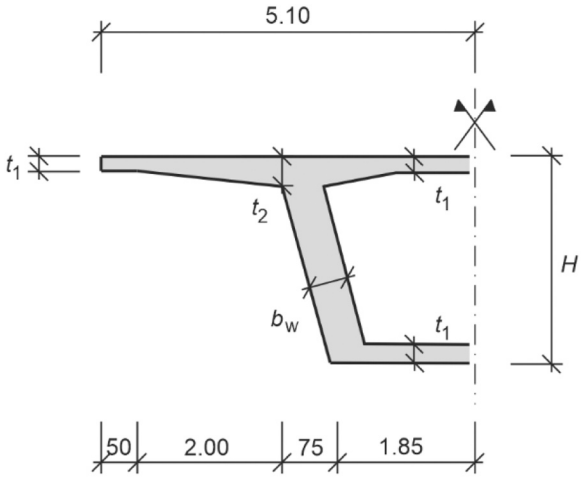

Fig. 4. Dimensions of the investigated segmental bridges according to [6].

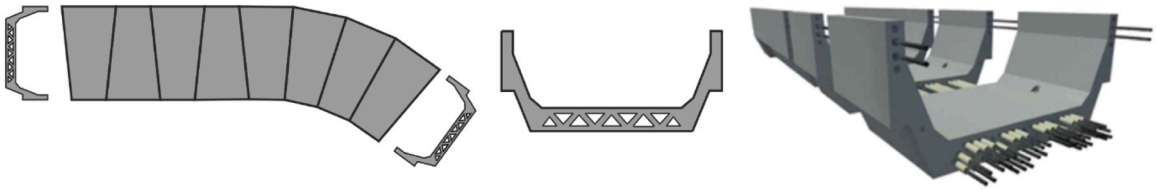

Fig. 3. Principle of flexible modular high-speed railway bridge made of UHPFRC [25].

Table 1
Concrete grades and dimensions of the investigated segmental bridges according to [6].

		C55/67	C80/95	C120/145	C180/217-H18	C180/217-H24
Height	H [m]	2.4	2.2	2.0	1.8	2.4
Web thickness	b_w [cm]	35	28	22	15	15
Slab thickness [cm]	t_1	20.0	18.0	16.0	12.0	12.0
	t_2	40.0	36.0	32.0	24.0	24.0
Area	A_c [m^2]	4.89	4.18	3.58	3.06	3.32
Span to depth ratio	L/H	18.8	20.5	22.5	25.0	18.8

regard to $f_{cd,fat}$ see Section 4.2). Conversely, this means that for the segmental bridges investigated in [6], the fatigue loading decreases or remains almost constant with increasing ratio between cyclic live loads and static dead loads. However, it should be taken into account that for all segmental bridges in [6], the concrete compressive strength was not really fully used or was used less and less with increasing concrete compressive strength ($\sigma_c < 0,45 \bullet f_{ck}$). An evaluation of the fatigue loading at shear stress level is not possible, since in [6] the shear stresses are not specified or corresponding load positions were not investigated.

3. Calculations

3.1. General

In order to investigate the issue of increasing fatigue loading in slender and filigree segmental structures with respect to both compressive stresses σ and shear stresses τ in more detail, own numerical investigations were carried out on segmental bridge superstructures with different concrete grades and varying cross-sectional dimensions or slendernesses. The starting point of the investigations presented is an externally prestressed road bridge with box-girder cross-section in cast-in-place concrete construction made of normal strength concrete C45/55 (M-NSC or monolithic reference bridge), which was essentially based on the design example from [30] (monolithic box-girder road bridge with external prestressing). The static system is a single-span girder supported in a statically determined longitudinal and transverse direction with an effective span of 80.00 m and a bridge length of 81.20 m, respectively (Fig. 5). Details of the load models and design approaches used are given in Section 3.3.

Based on the requirements of this bridge, further variants were developed and systematically optimized by segmentation, use of higher concrete grades and subsequent adjustment of the cross-section geometry:

- S-NSC: segmented variant made of C45/55
- S-HSC: segmented variant made of C80/95 with optimized cross-section
- S-UHPFRC-1: segmented variant made of C140 with optimized cross section
- S-UHPFRC-2: segmented variant made of C140 with optimized cross-section based on steel structures

For the variants S-UHPFRC-1 and S-UHPFRC-2, an ultra-high-performance concrete with a micro steel fiber content of 2.50% by volume was used according to [11]. The load-bearing effect of the fibers (post-cracking tensile strength of UHPFRC) was considered according to the draft of the DAfStb guideline for ultra-high-performance concrete [31]. The concrete cover was chosen to 4.5 cm for the normal and high strength concrete bridges (M-NSC, S-NSC and S-HSC) and to 2.0 cm for the UHPFRC bridges (S-UHPFRC-1 and S-UHPFRC-2) according to the design principles (see Section 2.2). The exposure classes were specified as XC4, XD1 and XF2 (see ZTV-ING [32]). Reinforcing steel grade B500 B was selected for the reinforcement and prestressing steel grade Y1770C was used for the prestressing.

The bridges were segmented by means of 28 standard segments, two end segments (S1 and S1') and two transverse bulkhead segments (S10 and S10'), each with a width of 2.50 m in the longitudinal direction of the bridge. The selected segment width is common in segmental bridge construction and ensures, among other things, transportability (e.g. [1, 6]). An additional standard segment (S17) with a width of 1.20 m was arranged in the middle of the bridge (see Fig. 6) to achieve the required bridge length of 81.20 m.

3.2. Calculation methods

The numerical calculations were carried out analogue to [6] (see Section 2.2.2) using the FE software package SOFISTIK 2022. In order to develop practical structural variants, the investigated variants were modeled using shell elements (QUAD-Element) as spatial numerical models and cable elements as tendons (Fig. 7). The element size of the shell elements was chosen to be 40 cm, whereby this was automatically reduced by SOFISTIK in the area of the segmental joints (for further

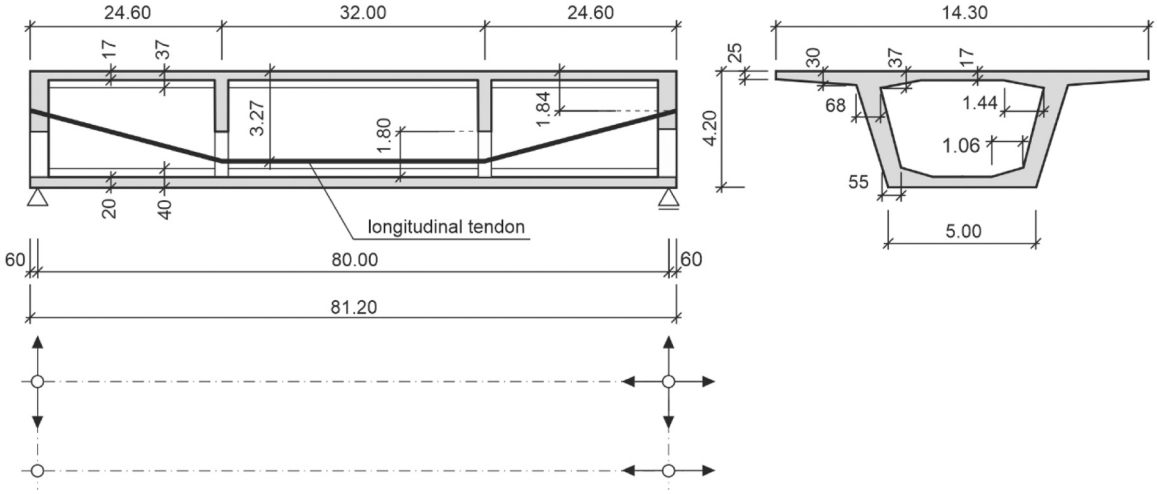

Fig. 5. Externally prestressed reference road bridge M-NSC with box girder cross-section based on the example according to [30] (exaggerated representation): longitudinal section (top left), support arrangement (bottom left) and cross-section (right) (all lengths in [m] and all cross-section dimensions in [cm]).

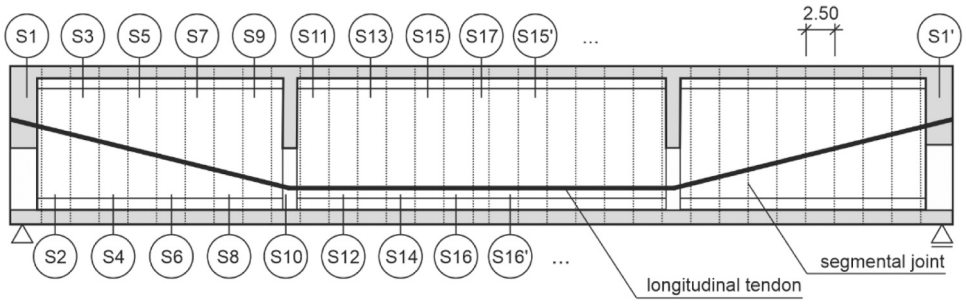

Fig. 6. Segmentation of the box girder bridge (longitudinal section).

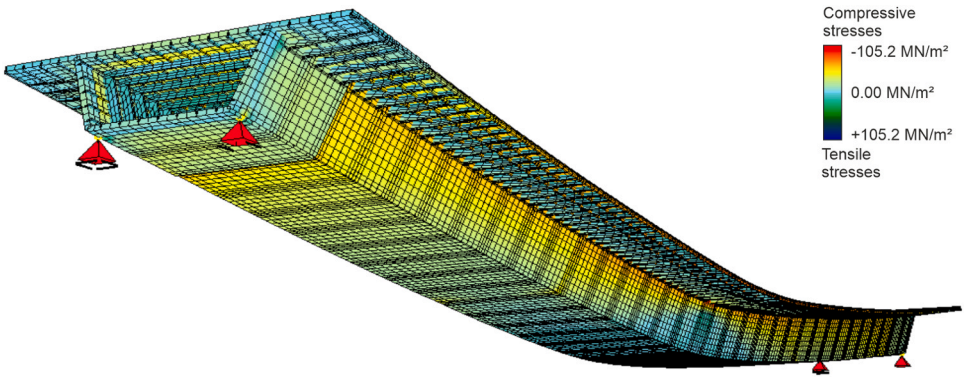

Fig. 7. FE-model of the segmental bridges S-UHPFRC-2 with calculated principal stresses and deflections in ULS (deflections shown exaggerated and end cross girders are hidden).

information on the element types and the meshing, see [33]).

The joints of the segmented variants were modeled using spring elements in accordance with [6] (see also [33]). For this purpose, a small distance was left between the segments (Fig. 8, left) in order to prevent unwanted meshing of the shell elements and to be able to arrange the spring elements. The spring elements can transmit both compressive and shear stresses, but fail under tensile loading. The stress-strain-diagrams of the spring elements are shown qualitatively in Fig. 8b) and c).

The corresponding spring parameters (force F and displacement u) were derived, verified and applied based on tests on keyed dry joints according to [34] for normal strength concrete, [35] for high strength concrete and [7,36,37] for ultra-high performance concrete. To account for the missing concrete cross-section, the spring stiffnesses were subsequently modified. Fig. 9 shows the centre of the span of the FE-model of the segmental bridge S-UHPFRC-2 (see also Fig. 7) with the calculated gaping of the segmental joints in ultimate limit state (ULS).

To consider the nonlinear load-bearing behavior, calculations were carried out using II. order theory. This allows, for example, an evaluation of the stability of the structure. The Reißner-Mindlin plate theory

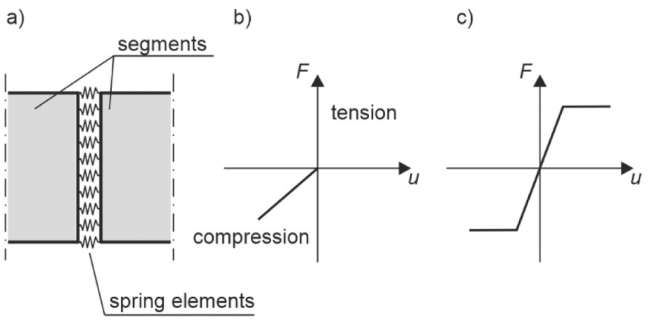

Fig. 8. Segmental joints: a) modelling principle, b) spring force-strain diagram for compressive forces and c) spring force-strain diagram for shear forces.

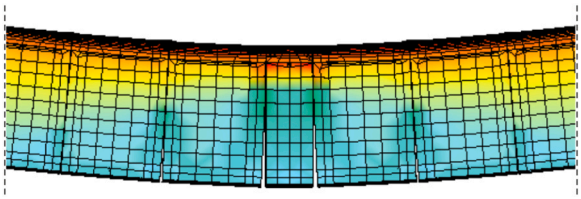

Fig. 9. Centre of the span of the FE model of the segmental bridges S-UHPFRC-2 with calculated gaping of the segmental joints as well as principal stresses and deflections in ULS (joint openings and deflections shown exaggerated).

was used to calculate the spatial FEM model in SOFISTIK 2022. In its assumption, the cross-section remains flat, but no longer perpendicular to the neutral axis. The same shape functions are used for the additional shear torsion as for the calculation of the displacements. The total torsion is then the sum of shear torsion and bending torsion. The shell elements used can also accurately capture disc bending without shear distortions using a non-conforming quadratic internal approach function and therefore have the correct stiffness. The bases for these calculation approaches are provided in [38,39] and [40]. In order to achieve convergence for the energy state of the system, the so-called line search method is used. Depending on the residual forces that occur, the load step width is reduced internally. If the iteration runs in the direction of an energy minimum, a new tangential stiffness is built up if necessary. The crack state of elements is recorded at a reduced stiffness. The FE model was verified by means of experimental and numerical investigations according to [6,34,41–48].

3.3. Design codes

The design of the bridge variants was based on EN 1992–2 +NA [49,50] or EN 1992–1-1 +NA [28,29] and the draft of the DAfStb guideline for ultra-high performance concrete [31]. The loads were applied in

accordance with EN 1991–2 +NA [26,27]. In order to reduce the computational effort, only one selected load position was investigated for load model 1 (Fig. 10) and for fatigue load model 3 (Fig. 11).

The additional construction loads were set identically for all variants. Although the time-dependent material behavior of the concrete and prestressing steel was not part of the investigations, the prestressing steel stresses were limited to the specified limit values of EN 1991–2 +NA, which in part also include time-dependent prestressing force losses. This also includes the limitation of the prestressing steel stresses without deduction of prestressing force losses to 65% of the prestressing steel tensile strength, which is on the safe side and leads to an increase of the prestressing steel cross section. Following [51], the respective prestressing was selected for the four segmented variants so that the concrete cross-sections have a compressive stress reserve of at least 1.00 MN/m^2 in the rare load combination, taking into account the stressing force dispersion. In addition, no minimum reinforcement (to avoid brittle failure) was taken into account for the segmented variants. In the case of the segmented variants, the gaping of the segmental joints corresponds to a failure with advance notice [34,47]. In addition to the required stress verifications in the serviceability limit state (SLS), the ultimate limit state (ULS) was also considered according to the above-mentioned codes. At ULS, the joint opening height was limited to 2/3 of the cross-section height (Fig. 9) according to [51,52]. The steel fibers used in the segmental UHPFRC variants can reduce the amount of reinforcing steel required, particularly when designing shear forces and torsion (e. g. 34). Due to the joint opening that occurs in the ULS, there are no significant crack widths in the segments themselves that could be limited by the fibers (e. g. [53–55]) - the main tensile stresses are assigned to the tendons. The stress increases occurring in the prestressing steel as a result of the joint opening and the reduction of the lever arm were directly recorded and taken into account due to the selected modeling and calculation method.

For the design of the cross-sections, the concrete compressive stresses in the rare action combination (SLS) were limited to $0,6 \bullet f_{ck}$, tacking into account the mean value of the prestressing force. This is based on the German National Annex to EN 1992–2, as in this case the fatigue verifications of concrete under compressive loading for road bridges can be considered to be fulfilled. A corresponding regulation can also be found in the French National Annex of EN 1992–2 for the design of UHPC [56]. The fatigue safety of the steel reinforcement was achieved by increasing the reinforcement content to such an extent that no fatigue problem exists.

Although the design was carried out in accordance with EN 1992–2 +NA and the DAfStb guideline, alternative approaches (e.g. [57–59] and [60]) provide more economical results in some cases, particularly for shear force design. However, these are generally only applicable to components with normal strength or high performance concrete. Design principles for UHPC components were analysed in [61], for example.

3.4. Bridges variants

Fig. 12 shows the cross-sections of the box-girder bridges developed in the course of the investigations with the numerical calculations. The S-NSC variant is based directly on the monolithic reference bridge M-NSC and only segments it. In the case of the S-HSC variant, the wall thicknesses of the box girder cross-section could be reduced by using HSC, since (in Germany) the minimum dimensions according to ZTV-ING [32] had to be adhered to and the full capacity of the HSC could therefore not be used. Since these minimum dimensions do not apply to UHPFRC (in Germany) and the UHPFRC requires higher strengths and a lower concrete cover (cf. [17,31]), the wall thicknesses could be further reduced in the S-UHPFRC-1 variant. However, the reduction in wall thicknesses was limited in this variant with respect to avoiding stability failure of the thin walls (buckling), although the very high strengths of the UHPFRC were not yet fully used. The avoidance of stability failure was based on [62] and [63]. The S-UHPFRC-1 variant is representative of the UHPFRC segmental bridges typically designed to date (e.g. [1,9,10,12,16]). Although these are designed to be significantly slimmer in direct comparison to structures made of normal strength or high strength concrete, they often fall far short of the capabilities of UHPFRC. As a result, these structures are much compacter and thicker than would be necessary at the material level. Consequently, the S-UHPFRC-2 variant was developed, the design being based on considerations according to [1] for extremely thin-walled bridge superstructure cross sections made of UHPFRC. The basic principle of the consideration is to make full use of the high strengths and durability of UHPFRC (to optimize material consumption) (e. g. [13,64,65]) and at the same time to avoid stability problems analogue to slender concrete compression members (e. g. [66,67]) or steel structures (e. g. [68]), which can fail far below their material load-bearing capacity due to stability failure. To avoid stability failure, the structure was designed with longitudinal and transverse ribs (Fig. 13), following common designs in steel construction. Furthermore, the cross-sectional height was reduced. This made it possible to use the high performance of the UHPFRC (Fig. 14). The fact that such thin-walled ribbed construction or complex shapes can be manufactured as prefabricated elements using UHPFRC is shown, among others, by the design of thin-walled, ribbed UHPFRC retaining walls [10,12] and thin-walled, ribbed parabolic trough and heliostat collectors [69,70]. For all investigated variants, the required verifications were performed in the SLS and ULS with the codes and described load positions given in Section 3.3.

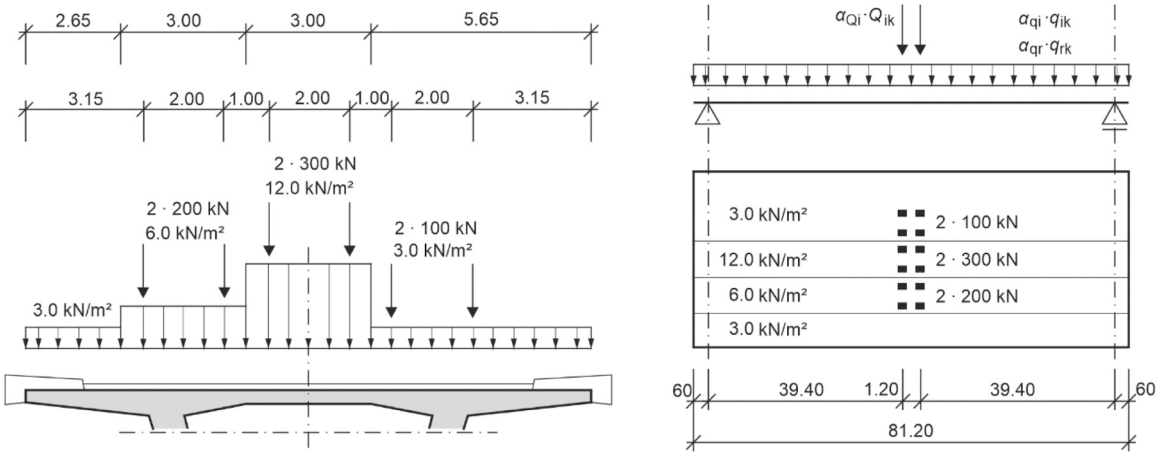

Fig. 10. Load positions of the load model 1 (LM1).

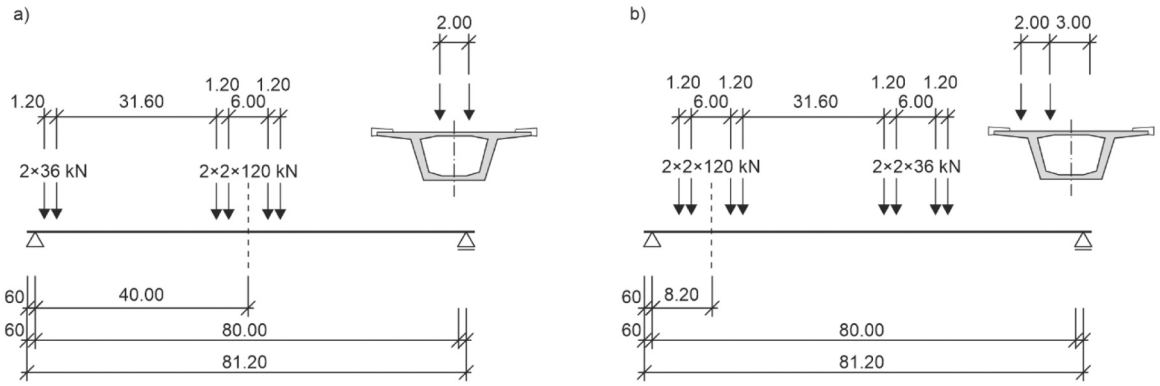

Fig. 11. Load positions of the fatigue load model 3 (FLM3) for a) bending and b) shear.

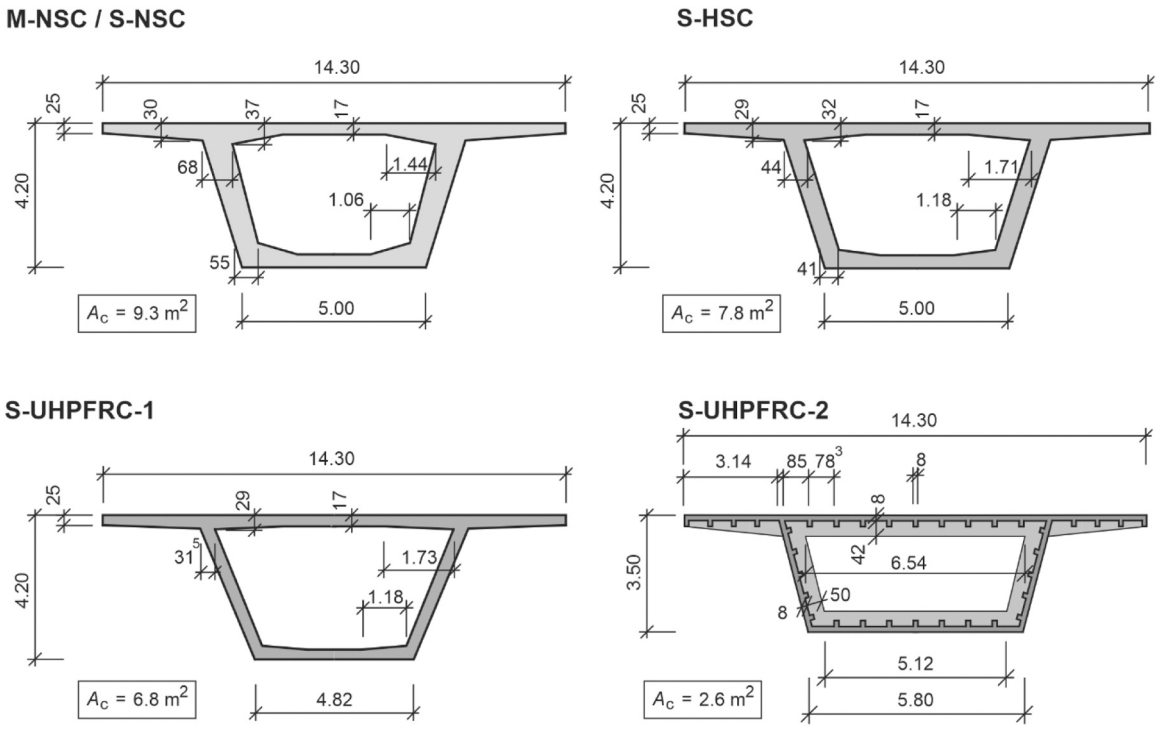

Fig. 12. Cross sections of the developed variants (all lengths in [m] and all cross-section dimensions in [cm]).

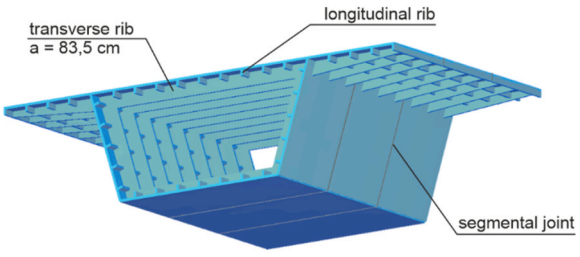

Fig. 13. Design of the segments of the variant S-UHPFRC-2 with longitudinal and transverse ribs.

In general, it can be summarized that the use of higher concrete strengths in the variants S-HSC as well as S-UHPFRC-1 and S-UHPFRC-2 allows a consistent reduction of the box girder wall thicknesses and thus slimmer and thinner-walled cross sections. When looking at the ratio of the height H to the web thickness b_w of the individual bridge cross-sections (S-NSC: $H/b_w = 4.2/0.55 = 7.6$; S-HSC: $H/b_w = 4.2/0.41 = 10.2$; S-UHPFRC-1: $H/b_w = 4.2/0.30 = 14.0$; S-UHPFRC-2: $H/b_w = 3.5/0.08 = 43.8$), the variant S-UHPFRC-2 with a H/b_w ratio of 43.8 shows by far the greatest cross-sectional slenderness, so that it is considered thin-walled in this article. The volumes and weights of the construction materials (concrete, reinforcing steel, prestressing steel and steel fibers) and their changes are listed in Table 2 as a function of the individual variants – the monolithic bridge M-NSC is used as a reference for the percentage changes.

Table 2 shows that the S-HSC variant saves 14.8% of the amount of concrete compared to the monolithic reference bridge M-NSC, while the S-UHPFRC-1 variant saves more than 30% and the S-UHPFRC-2 variant even 65%. The increase of 0.2% for the segmented variant S-NSC results from the fact that less reinforcing steel or flexural reinforcement has to be used compared to the monolithic reference bridge M-NSC. Consideration of the two NSC variants shows that the amount of reinforcing steel can be drastically reduced by segmentation, since significant parts of the longitudinal reinforcement, which are necessary for the ULS as well as for the crack width limitation, are eliminated or compensated by a slightly higher prestress. The saving in the amount of reinforcing steel

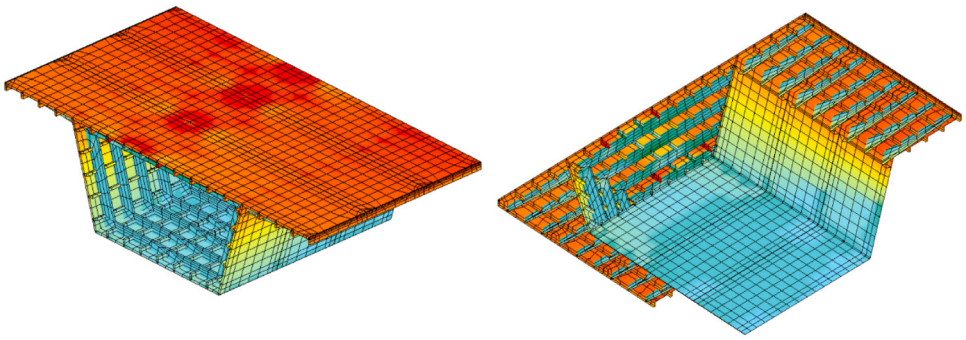

Fig. 14. FE model of three standard segments of the variant S-UHPFRC-2 with calculated principal stresses in ULS.

Table 2
Overview of variants and their characteristic features (changes relative to M-NSC).

Variant	Construction method	Building materials	Volume	Weight	Change
M-NSC	monolithic	concrete (C45/55)	794.4 m^3	1866.9 t	/
		reinforcing steel (B500 B)	8.1 m^3	63.4 t	/
		prestressing steel (Y1770C)	9.1 m^3	71.0 t	/
S-NSC	segmented	concrete (C45/55)	796.3 m^3	1871.4 t	+ 0.2%
		reinforcing steel (B500 B)	6.2 m^3	48.5 t	- 23.5%
		Prestressing steel (Y1770C)	10.9 m^3	85.3 t	+ 20.1%
S-HSC	segmented	concrete (C80/95)	676.7 m^3	1590.2 t	- 14.8%
		reinforcing steel (B500 B)	6.0 m^3	47.0 t	- 25.9%
		prestressing steel (Y1770C)	9.7 m^3	76.3 t	+ 7.5%
S-UHPFRC-1	segmented	concrete (C140)	554.6 m^3	1303.3 t	- 30.2%
		reinforcing steel (B500 B)	5.4 m^3	42.2 t	- 33.4%
		prestressing steel (Y1770C)	8.0 m^3	62.5 t	- 12.0%
		steel fibers (2,50 Vol.-%)	14.4 m^3	112.7 t	/
S-UHPFRC-2	segmented / longitudinal and transverse ribs	concrete (C140)	278.6 m^3	654.7 t	- 64.9%
		reinforcing steel (B500 B)	3.0 m^3	23.6 t	- 62.8%
		prestressing steel (Y1770C)	8.4 m^3	65.7 t	- 7.5%
		steel fibers (2,50 Vol.-%)	7.2 m^3	56.7 t	/

is around 23%. For the S-HSC variant, the saving in the amount of reinforcing steel is about 26%. For the UHPFRC variants, the saving is about 33% (S-UHPFRC-1) and about 63% (S-UHPFRC-2). For these two variants, the saving is also largely due to the post-cracking tensile strength of the UHPFRC (crack-bridging effect of the steel fibers). On the other hand, compared with the monolithic initial variant M-NSC, the segmental variants S-NSC and S-HSC basically increase the amount of prestressing steel required. This is due to the fact that, because of the segmentation of the structure and the joints, the tendons have to transfer considerably larger load components that are transferred by the reinforcing steel in the monolithic initial variant (see also compressive stress reserve of at least 1.00 MN/m^2). Therefore, the quantities of prestressing steel of the S-NSC and S-HSC variants increase by 20% and approx. 7%, respectively, compared to the initial variant, even though almost one seventh of the dead weight could already be saved in the S-HSC variant. Only with the UHPFRC variants can prestressing steel be saved due to the savings in concrete and the associated reduction in dead weight. Compared with the initial M-NSC variant, 12% prestressing steel can be saved in variant S-UHPFRC-1 and approx. 8% in variant S-UHPFRC-2. The lower saving potential of variant S-UHPFRC-2 compared with variant S-UHPFRC-1 can be explained by the smaller lever arm resulting from the reduction in the cross-section height.

The material savings achieved in the course of cross-section optimization not only have various advantages in terms of life cycle assessment, but also from a structural design perspective. The savings reduce the dead weight of the structures, resulting in a lower design load. On the one hand, this enables easier transport and installation of the precast segments, which in turn leads to reduced construction times (e.g. [34,47,52]). On the other hand, the supports and the bridge substructures (piers and abutments as well as foundations) can be designed smaller. All this leads to resource savings and economic efficiency as well as sustainability. A life cycle assessment including an explicit consideration of the resource consumption of the individual bridge variants can be found in [8]. All this shows that thin-walled UHPFRC segmental bridges are a sustainable alternative to conventionally constructed bridges made of NSC.

4. Fatigue loading

4.1. General

In order to obtain a better understanding of the load conditions of the individual bridge variants, the ratio of live loads (LL) to the total loads (TL) was determined (Fig. 15). The total loads (TL) represent the sum of the dead loads (see Table 2), the additional construction loads and the applied live loads (see load model LM1 and FLM3 in Section 3.3). Fig. 15 clearly shows that the proportion of live loads of the load model LM1 (Fig. 12, left) increases slightly and linerarly for the variants M-NSC, S-NSC, S-HSC and S-UHPFRC-1 and amounts to approx. 30% of the total loads, while for the material-optimized variant S-UHPFRC-2 it accounts for almost 50% of the total loads. This enormous increase in the proportion of live loads in the total loads can also be seen in the evaluation with the load model FLM3 (Fig. 15, right), although the absolute proportion of the load is lower. This is due to the lower loads of the load model FLM3 compared to the load model LM1.

Since the segmental joints represent discontinuity areas in segmental bridges (see also Section 1) and their load-bearing capacity is of decisive importance for the load-bearing safety of the entire segmental structure, the compressive stresses σ_c and shear stresses τ_c in the relevant segmental joints (in the center of the span for the compressive stresses and in the support area for the shear stresses) are examined in more detail for the following evaluations. For an interpretation of the results

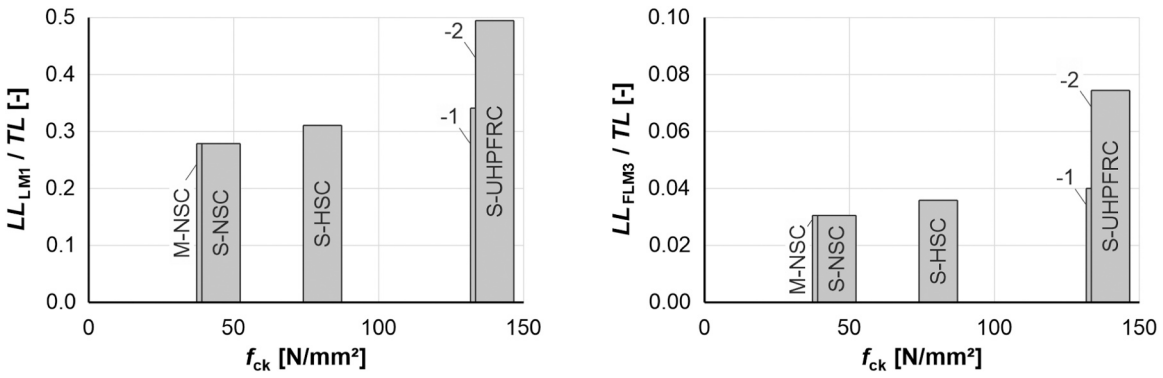

Fig. 15. Proportion of live loads (LL) of the load model LM1 (left) and the load model FLM3 (right) in relation to the total loads (TL) as a function of the characteristic concrete compressive strength f_{ck} of the individual variants.

and the fatigue loading, design elements were used that can integrate the area element stresses and internal forces over the cross-section area of the box girder to form beam stresses or beam internal forces (Fig. 16). Since the values are absolute values and can only be compared with each other to a limited extent, the stresses in the evaluations in Sections 4.2 and 4.3 are related to the design fatigue reference strengths of the concrete.

4.2. Compressive stresses

The evaluation of the fatigue loading of the compressive stresses of the individual variants was carried out in such a way that the compressive stresses σ_c (maximum stress $\sigma_{c,max}$, minimum stress $\sigma_{c,min}$ and stress range $\Delta\sigma_c$) were evaluated at the service load level (frequent load combination) in the center of the span at the bottom of the cross-section and related to the fatigue compressive strength of concrete $f_{cd,fat}$ (cf. Eq. 1 and Eq. 2) (Table 3 and Fig. 17). The design fatigue reference strength of concrete under compression was calculated for normal and high strength concretes in accordance with [28,29] to be

$$f_{cd,fat} = 1.0 \bullet \beta_{cc}(t_0) \bullet f_{cd} \bullet (1 - f_{ck}/250) \quad (1)$$

and for ultra-high performance concrete according to the draft of the DAfStb guideline for ultra-high performance concrete [31] to be

$$f_{cd,fat} = 0.8 \bullet \beta_{cc}(t_0) \bullet f_{cd} \bullet (1.1 - f_{ck}/500) \quad (2)$$

Where $\beta_{cc}(t_0)$ is the coefficient for concrete strength at first load application and set here to 1.0, f_{cd} is the design value of concrete compressive strength with $f_{cd} = \alpha_{cc} \bullet f_{ck}/\gamma_c$, where α_{cc} is the coefficient taking account of long term effects and is 0,85, f_{ck} is the characteristic compressive cylinder strength of concrete at 28 days and γ_c is the partial factor for concrete and is 1.50.

If the absolute values of the normal stresses $\sigma_{c,max}$, $\sigma_{c,min}$ and $\Delta\sigma_c$ of the individual bridge variants are analysed (Table 3), it can be seen that these increase with increasing concrete grade. This is due to the fact that the cross-sectional area A_c of the bridge variants (see Fig. 12) decreases with increasing concrete quality. The difference of the normal stresses $\sigma_{c,max}$ and $\sigma_{c,min}$ between the M-NSC and S-NSC variants, on the other hand, results from the significantly higher prestressing of the segmental bridge S-NSC (see Table 2). This does not include the stress range $\Delta\sigma_c$, as there is (almost) no difference in the dead weight of these two bridges.

The evaluations of the related compressive stresses of the variants S-NSC, S-HSC and S-UHPFRC-1 (Table 3 and Fig. 17) show that with increasing concrete grade or slimmer and thus lighter bridge, the related maximum stress $\sigma_{c,max}/f_{cd,fat}$ and the related stress range $\Delta\sigma_c/f_{cd,fat}$ decrease. This is comparable to the evaluations of the compressive stresses of the investigations according to [6] (see Section 2.2.2) and can again be attributed to the incomplete use of the concrete compressive strength for S-HSC and S-UHPFRC-1 (see Section 3.4). In contrast, for the S-UHPFRC 2 variant, in which the strength and durability of UHPFRC were consistently exploited by a material-appropriate design, there is an increase in the related maximum stress $\sigma_{c,max}/f_{cd,fat}$ (factor ≈ 1.4), in the related minimum stress $\sigma_{c,min}/f_{cd,fat}$ (factor ≈ 1.3), and in the related stress range $\Delta\sigma_c/f_{cd,fat}$ (factor ≈ 1.6) (factors related to S-NSC), even though the cross sections or the dry joints are fully compressed under service load levels. This increase can be attributed to the larger ratio of live loads (LL) to the total loads (TL) of this variant compared to the other variants (Fig. 14).

When designing the cross-sections of the individual variants, the concrete compressive stresses in the rare combination of actions (SLS) were limited to $0.6 \bullet f_{ck}$ in accordance with the German National Annex to EN 1992–2, thus indirectly verifying the fatigue of concrete under compressive loading (see Section 3.3). Despite compliance with this general normative regulation, the results show that very high upper and lower related stresses can occur in very slender and filigree bridge cross-sections and thus a fatigue problem of the concrete can exist and this general normative regulation may not always be on the safe side.

Table 3 and Fig. 17 (left), also show that for the S-UHPFRC-2 variant, the maximum compressive stress $\sigma_{c,max}$ is 86% and the minimum compressive stress $\sigma_{c,min}$ is 78% of the fatigue compressive strength of

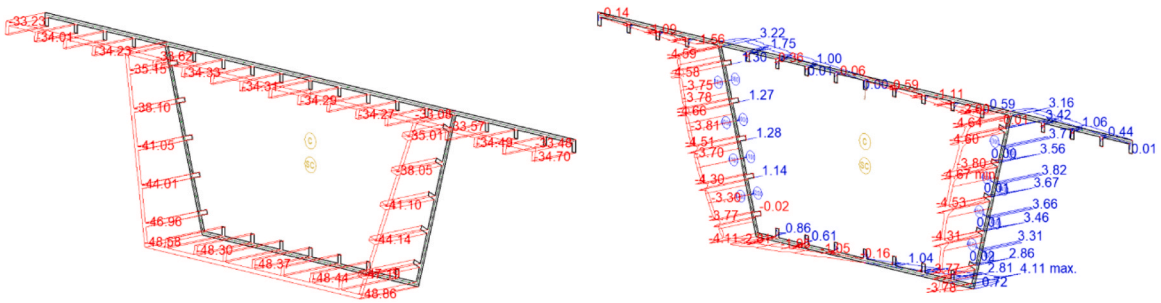

Fig. 16. Example output of compressive stresses σ_c in the center of the span (left) and shear stresses τ_c in the support area (right) of the variant S-UHPFRC-2.

Table 3
Maximum stresses $\sigma_{c,max}$, minimum stresses $\sigma_{c,min}$ and stress ranges $\Delta\sigma_c$ as well as fatigue compressive strength of concrete $f_{cd,fat}$ and related compressive stresses of the individual variants.

	$\sigma_{c,max}$ [MN/m²]	$\sigma_{c,min}$ [MN/m²]	$\Delta\sigma_c$ [MN/m²]	$f_{cd,fat}$ [MN/m²]	$\sigma_{c,max}$ / $f_{cd,fat}$ [-]	$\sigma_{c,min}$ / $f_{cd,fat}$ [-]	$\Delta\sigma_c$ / $f_{cd,fat}$ [-]
M-NSC	4.9	3.8	1.0	20.9	0.23	0.18	0.05
S-NSC	13.2	12.2	1.0	20.9	0.63	0.58	0.05
S-HSC	13.7	12.6	1.1	30.8	0.44	0.41	0.04
S-UHPFRC-1	16.3	15.0	1.3	52.0	0.31	0.29	0.03
S-UHPFRC-2	44.9	40.4	4.1	52.0	0.86	0.78	0.08

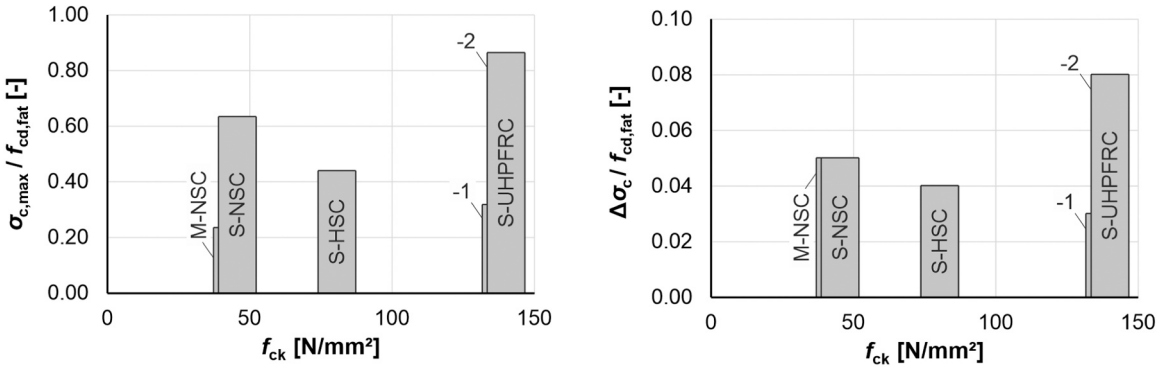

Fig. 17. Related maximum stress $\sigma_{c,max}/f_{cd,fat}$ (left) and related stress range $\Delta\sigma_c/f_{cd,fat}$ (right) as a function of the characteristic concrete compressive strength f_{ck} of the individual variants.

concrete $f_{cd,fat}$ according to the DAfStb guideline (cf. Eq. (2)). These stresses could possibly be critical or lead to failure of the segmental bridge. Investigations according to [11,46] on externally prestressed monolithic and segmental UHPFRC beams with thin-walled box girder cross-section under monotonically increasing torsional loading and monotonically increasing combined bending, shear and torsional loading have shown that the principal compressive stresses may not exceed approximately 50% of the compressive strength of the UHPFRC. Beyond this, brittle failure of the UHPFRC occurs (Fig. 18).

It is currently unclear whether such a failure occurs under fatigue loading and to what extent the compressive strength of the concrete of fatigue-loaded (segmental) UHPFRC beams can be stressed. As already mentioned in Section 1, when designing segmental concrete towers of hybrid wind turbines in accordance with DIN 18088–2 [24], a fatigue design of the concrete under compressive stress must be carried out and an increased compressive stress of 15% or 35% must be applied. However, studies on the fatigue behaviour of the material UHPFRC under compressive stresses are available and can be found, for example, in [71–73]. These investigations show that UHPFRC does not exhibit any significant difference compared to NSC and HPC at the same related stresses ($\sigma_{c,max/min}/f_{cd,fat}$) under fatigue loading under compression and that the corresponding S/N curves are (almost) independent of the concrete strength class.

4.3. Shear stresses

Furthermore, the shear stresses τ_c (maximum stress $\tau_{c,max}$, minimum stress $\tau_{c,min}$ and stress range $\Delta\tau_c$) in the serviceability limit state (frequent load combination) in the support area were evaluated for the individual bridge variants (Table 4). Deviating from the compressive stresses, the shear stresses were not related to the design fatigue reference strength of concrete under compression $f_{cd,fat}$, but to the design fatigue reference strength of concrete under tension $f_{ctd,fat}$. The relation to the concrete tensile strength is based on the following: In segmental structures, the keyed dry joints represent discontinuity areas and their load-bearing capacity is essential for the load-bearing capacity of the

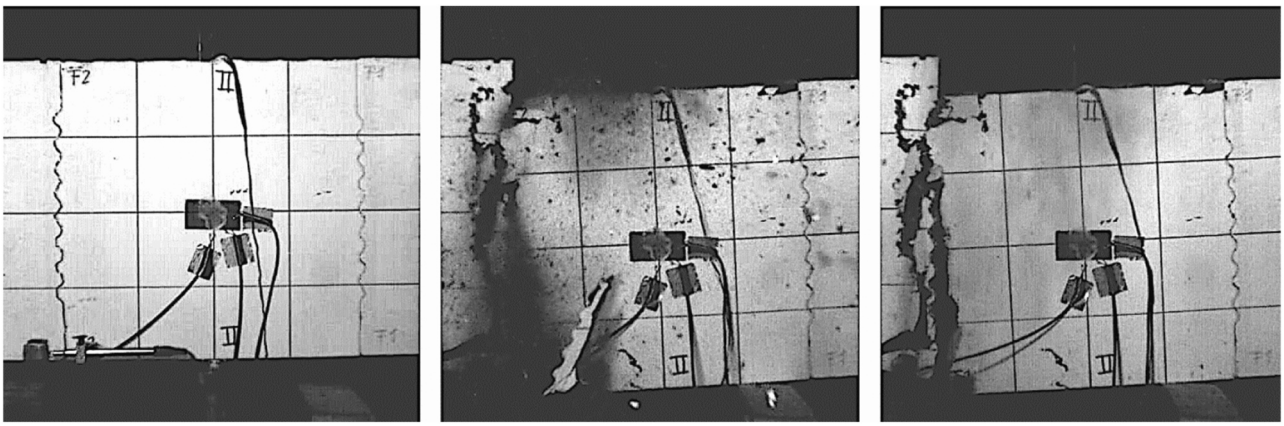

Fig. 18. Brittle failure of the concrete of a prestressed UHPFRC segmental beam (V10) under combined bending, shear and torsional loading (images from a high-speed camera) according to [11].

Table 4
Maximum stresses $\tau_{c,max}$, minimum stresses $\tau_{c,min}$ and stress ranges $\Delta\tau_c$ as well as concrete tensile fatigue strength $f_{ctd,fat}$ and related shear stresses of the individual variants.

	$\tau_{c,max}$ [MN/m²]	$\tau_{c,min}$ [MN/m²]	$\Delta\tau_c$ [MN/m²]	$f_{ctd,fat}$ [MN/m²]	$\tau_{c,max}$ / $f_{ctd,fat}$ [-]	$\tau_{c,min}$ / $f_{ctd,fat}$ [-]	$\Delta\tau_c$ / $f_{ctd,fat}$ [-]
M-NSC	2.1	1.8	0.3	1.8	1.18	1.01	0.17
S-NSC	1.6	1.3	0.3	1.8	0.89	0.72	0.17
S-HSC	2.0	1.6	0.4	2.3	0.87	0.70	0.17
S-UHPFRC-1	2.6	2.0	0.6	3.7	0.70	0.54	0.16
S-UHPFRC-2	6.0	3.0	3.0	3.7	1.62	0.81	0.81

entire segmental structure. The failure of keyed dry joints under monotonically increasing shear loading is characterized by shearing of the profiling (shear keys) and is thus directly dependent on the concrete tensile strength (Fig. 19, see also [74,75]). Consequently, it can be assumed that the fatigue failure of keyed dry joints under shear loading is also directly dependent on the concrete tensile strength. However, as far as the authors are aware, there have been no studies to date on the load-bearing behavior of keyed dry (UHPFRC) joints under fatigue (shear) loading. Nevertheless, (initial) studies on the fatigue behaviour of the material UHPFRC under tensile stresses are available and can be found, for example, in [18,76–79]. On the one hand, the investigations show that the micro steel fibers have a stabilising effect on micro-crack formation. On the other hand, micro steel fibers can also have a crack-initiating effect. The fatigue behaviour of the material UHPFRC under tensile stresses has not yet been clearly clarified and is still the subject of research.

Since EN 1992–2 +NA [49,50] or EN 1992–1-1 +NA [28,29] and the draft of the DAfStb guideline for ultra-high performance concrete [31] do not contain any information on the determination of the fatigue tensile strength of concrete $f_{ctd,fat}$, these were determined according to Model Code 2010 [80] and also assumed for UHPFRC:

$$f_{ctd,fat} = f_{ctk;0,05} / \gamma_{c,fat} \tag{3}$$

Where $f_{ctk;0,05}$ is the characteristic axial tensile strength of concrete and $\gamma_{c,fat}$ the partial factor for fatigue of concrete with $\gamma_{c,fat} = 1.50$. This concrete tensile fatigue strength $f_{ctd,fat}$ according to Model Code 2010 strictly applies only in embedded form in different verification methods (Level II and III) of concrete fatigue. The verification-specific modifications of the concrete tensile fatigue strength $f_{ctd,fat}$ are made in combination with a further reduction coefficient (Level II), which is then used to determine a lower limit value, or by specifying a conservatively held specific tolerable number of load cycles (Level III). Due to the lack of other normative approaches for determining the concrete tensile fatigue strength $f_{ctd,fat}$, the concrete tensile fatigue strength $f_{ctd,fat}$ of the individual bridge variants was determined in the following according to Eq. (3), although it is – in the opinion of the authors – a very progressive value without the addition of modifications (i.e. standing alone).

Fig. 20 shows the related maximum stress $\tau_{c,max}/f_{ctd,fat}$ (left) and the related stress range $\Delta\tau_c/f_{ctd,fat}$ (right) as a function of the characteristic concrete compressive strength f_{ck} of the individual variants.

When analysing the absolute values of the shear stresses $\tau_{c,max}$, $\tau_{c,min}$ and $\Delta\tau_c$ of the bridge variants (Table 4), it can be observed that these increase with increasing concrete grade. This is due to the fact that the wall thickness of the webs of the individual bridge cross-sections (see Fig. 12) decreases with increasing concrete grade. The difference of the shear stresses $\tau_{c,max}$ and $\tau_{c,min}$ between the M-NSC and S-NSC variants results from the significantly higher prestressing of the S-NSC segmental bridge (see Table 2). The higher prestressing results in a larger shear force resulting from the prestressing, which counteracts the shear force from the self-weight and traffic load. The stress range $\Delta\tau_c$ is not affected by this, as the dead weight of the M-NSC and S-NSC bridges (almost) does not differ.

The evaluations (Table 4 and Fig. 20) show that the related maximum stress $\tau_{c,max}/f_{ctd,fat}$, the related minimum stress $\tau_{c,min}/f_{ctd,fat}$, and the related stress range $\Delta\tau_c/f_{ctd,fat}$ remain approximately constant for the variants S-NSC, S-HSC and S-UHPFRC-1, but lead to a huge increase in the case of variant S-UHPFRC-2 - in which the strengths and durability of the UHPFRC have been consistently exploited by a material-appropriate design (cf. Fig. 14). Compared to the variants M-NSC, S-NSC, S-HSC and S-UHPFRC-1, factors of up to 1.8 (related maximum stress), 1.1 (related minimum stress) and 4.8 (related stress range), respectively, are obtained for variant S-UHPFRC-2, even though the cross sections or the dry

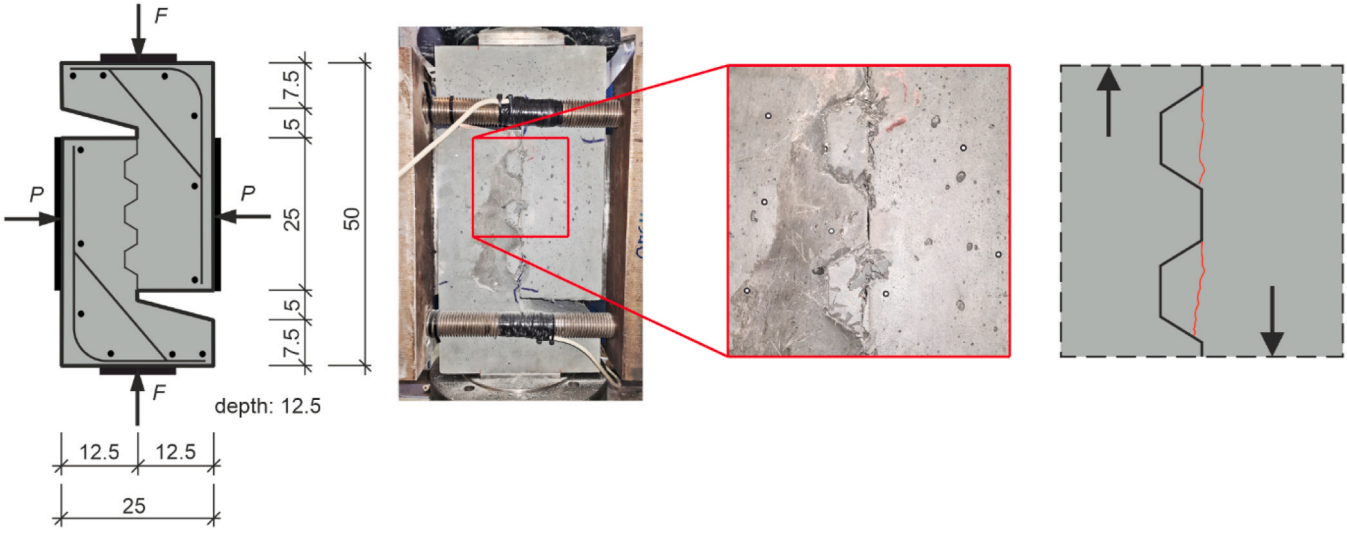

Fig. 19. Push off test with keyed dry joint made of UHPFRC under monotonically increasing shear loading: principle sketch (left), test specimen in the test setup after the test (center left), enlarged section of the failure area or sheared shear keys (center right) and schematic crack pattern (right).

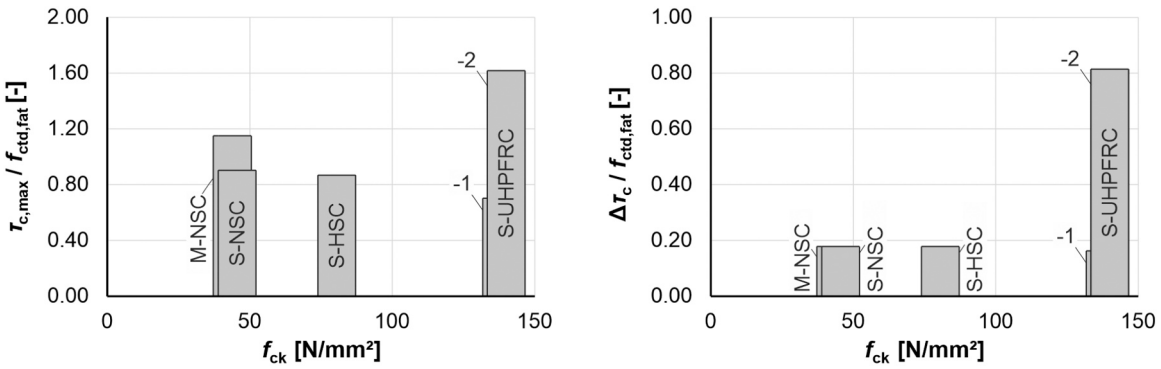

Fig. 20. Related maximum stress $\tau_{c,max}/f_{ctd,fat}$ (left) and related stress range $\Delta\tau_c/f_{ctd,fat}$ (right) as a function of the characteristic concrete compressive strength f_{ck} of the individual variants.

joints are completely compressed at service load levels. The increase of the shear stresses is thus comparable to the results according to [25] (amplification of the stirrups by a factor of 1.5 in the fatigue check of the shear reinforcement of the modular high-speed railway bridge made of UHPFRC, cf. Section 2.2.1). The enormous increase is mainly due to the increasing influence of the LL/TL ratio of the lightweight filigree segmental bridge S-UHPFRC-2 (= large ratio between cyclic live loads and static dead loads cf. Fig. 15). Another effect is that the concrete tensile strength does not increase proportionally to the concrete compressive strength with increasing concrete grades, but decreases from about 10% of the compressive strength for normal strength concrete (C20/25: 20 N/mm^2 to 2.2 N/mm^2, according to [49]) to about 5% of the compressive strength for ultra-high performance concrete (C175/190: 175 N/mm^2 to 9.4 N/mm^2, according to [31] (Fig. 21).

It can also be seen from Table 4 or Fig. 20 (left), that the maximum stress $\tau_{c,max}$ is about 70% to 90% (M-NSC, S-NSC, S-HSC and S-UHPFRC-1) or about 160% (S-UHPFRC-2) of the design value of the concrete tensile fatigue strength $f_{ctd,fat}$ according to Model Code 2010 (Eq. (3)). This is to be considered critical especially for the load-bearing capacity of the keyed dry joints of variant S-UHPFRC-2. However, it must be taken into account here that the joints are completely under compressive stresses in the serviceability limit state and thus a multi-axial stress state is available in the joint area and, in turn, an increased concrete tensile strength compared to the unconfined concrete tensile strength [81]. However, in the investigations carried out here – due to the smeared modeling of the segmental joints by means of spring elements (see Section 3.2) – design-related effects, such as notch stresses occurring at the corners of the joint profiling (see Figs. 18 and 19), were not taken into account, so that these effects could cancel out the slightly higher multi-axial concrete tensile strength and thus joint failure under fatigue loading cannot be excluded. In addition, it must be taken into account that the fatigue tensile strength of concrete $f_{ctd,fat}$ (Eq. (3)) is a very progressive value – according to the authors – and that $f_{ctd,fat}$ may be much lower than the value used here. In the case of the S-UHPFRC-2 variant, this must also be considered critical with respect to the minimum stress $\tau_{c,min}$ (81%) as well as the stress range $\Delta\tau_c$ (81%), as these are very close to the value of the fatigue tensile strength of concrete $f_{ctd,fat}$. In contrast, the minimum stresses $\tau_{c,min}$ of the variants S-NSC, S-HSC and S-UHPFRC-1 reach only about 50% to 75% of the value of the fatigue tensile strength of concrete $f_{ctd,fat}$ and the stress ranges $\Delta\tau_c$ remain at a very low level (< 1.0 N/mm^2 or maximum 17% of the fatigue tensile strength of concrete), so that fatigue failure can probably be excluded for these variants.

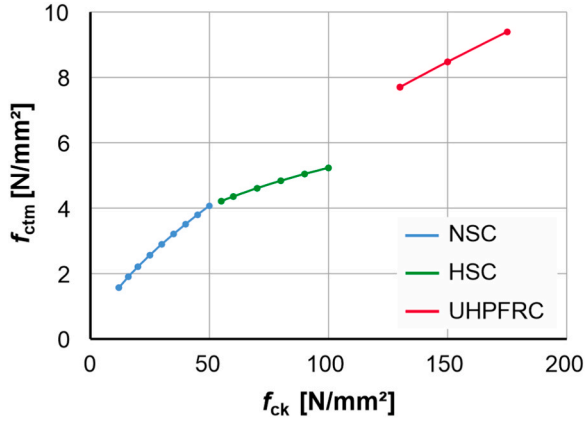

Fig. 21. Mean value of axial tensile strength of concrete f_{ctm} as a function of the characteristic concrete compressive strength f_{ck} according to EN 1992–1-1 [28] for normal strength (NSC) and high strength concrete (HSC) (blue and green line) as well as according to the draft of the DAfStb guideline [31] for ultra-high performance concrete (UHPFRC) (red line).

5. Conclusions and outlook

In order to meet the need for replacement of the many defective reinforced and prestressed concrete bridges in the future with sustainable, resource-efficient and material-appropriate alternatives, UHPFRC segmental bridge construction offers a very promising approach. However, due to the slenderness of these thin-walled structures and the associated lower loads from dead weight, live loads could gain influence in terms of fatigue loads. In order to investigate this issue in more detail, relevant findings from the literature were researched and analyzed. Furthermore, FE calculations were carried out on segmental bridges with box girder cross-section under variation of concrete strength (NSC, HSC and UHPFRC), where the cross-section dimensions were optimized and the fatigue loading was evaluated. Based on the investigations, the following conclusions could be drawn:

1. By using higher concrete strengths, the required construction materials and thus the dead weight of the bridges can be drastically reduced. If UHPFRC is used instead of NSC, savings of up to 65% for concrete, up to 63% for reinforcement steel and up to 8% for prestressing steel can be achieved (bridge S-UHPFRC-2 compared to bridge M-NSC).
2. The evaluation of the ratio of the live loads (LL) to the total loads (TL) showed that the proportion of the live loads in the M-NSC, S-NSC, S-HSC and S-UHPFRC-1 bridge variants is approx. 30% of the total loads, whereas in the material-optimised S-UHPFRC-2 bridge variant it accounts for almost 50% of the total loads and therefore higher fatigue loads should tend to occur in this variant.
3. For the conventional bridge variants M-NSC and S-NSC made of normal strength concrete, the related maximum stresses $\sigma_{c,max}/f_{cd,fat}$ and $\tau_{c,max}/f_{ctd,fat}$, the related minimum stresses $\sigma_{c,max}/f_{cd,fat}$ and $\tau_{c,min}/f_{ctd,fat}$, and the stress ranges $\Delta\sigma_c/f_{cd,fat}$ and $\Delta\tau_c/f_{ctd,fat}$ are in a

non-critical range. This finding is analogous to previous reinforced concrete and prestressed concrete bridges, where fatigue loading is rarely a problem with respect to the concrete, especially since a compact design means that the cyclic live loads are relatively low compared to the static dead loads.

4. The bridge variants S-HSC and S-UHPFRC-1 made of (ulta-) high-performance concretes did not exhibit increased fatigue loading despite the thin-walled cross-sections, as the concrete was not fully used in these variants and the live loads amounted to around 30% of the total loads.
5. However, in the thin-walled bridge variant S-UHPFRC-2, in which the strength and durability of the UHPFRC was consistently used, increased fatigue stresses occurred. Compared to the monolithic reference bridge M-NSC, an increase of the related maximum stress $\sigma_{c,max}/f_{cd,fat}$ by a factor of 1.4, of the related minimum stress $\sigma_{c,min}/f_{cd,fat}$ by a factor of 1.3, and of the related stress range $\Delta\sigma_c/f_{cd,fat}$ by a factor of 1.6 was observed for the S-UHPFRC-2 variant in the compressive stresses. The shear stresses also show an enormous increase with factors of 1.8 for the related maximum stress $\tau_{c,max}/f_{ctd,fat}$, 1.1 for the related minimum stress $\tau_{c,min}/f_{ctd,fat}$, and 4.8 for the related stress range $\Delta\tau_c/f_{ctd,fat}$.

Based on the results obtained, it can be concluded that fatigue problems of the concrete under compression or shear loading can occur in material-optimized and thus thin-walled UHPFRC segmental bridges, similar to thin-walled segmental concrete towers of hybrid wind turbines. In particular, the shear resistance of the keyed dry joints to fatigue loading should be investigated in more detail, since, on the one hand, the failure of the keyed dry joints (under monotonically increasing load) is directly dependent on the concrete tensile strength and, on the other hand, design-related effects, such as notch stresses occurring at the corners of the joint profiling, could lead to a reduction in the load-bearing capacity under fatigue loading and thus to premature failure of the keyed dry joints. Initial investigations into this were recently carried out at the Institute of Concrete Construction at Leibniz University Hannover.

Funding

This research did not receive any specific grant from funding agencies in the public, commercial, or not-for-profit sectors.

CRediT authorship contribution statement

Marvin Wilkening: Writing - original draft, Investigation, Formal analysis, Data curation, Validation. **Linus Joachim:** Writing - original draft, Formal analysis, Visualisation. **Vincent Oettel:** Writing - review & editing, Supervision, Resources, Methodology, Conceptualisation.

Declaration of Competing Interest

The authors declare that they have no known competing financial interests or personal relationships that could have appeared to influence the work reported in this paper.

Data Availability

Data will be made available on request.

Acknowledgements

The authors would like to thank Christian Clergue, Ph. D. for providing Fig. 2, right and Dipl.-Ing. Dr. techn. Michael Reichel for providing the illustrations in Fig. 3.

References

[1] Forman P, Glock C, Mark P. Schnelles Bauen – motivation, historie und Konzepte. Sonderheft S2 Beton- und Stahlbetonbau 2021;116:2–11. https://doi.org/10.1002/best.202100064.
[2] Omar T, Nehdi ML. Condition assessment of reinforced concrete bridges: current practice and research challenges. Infrastructures 2018 2018;3(3):36. https://doi.org/10.3390/infrastructures3030036.
[3] Figueiredo, E.; Moldovan, I.; Marques, M.B. (2013) Condition Assessment of Bridges: Past, Present and Future – A Complementary Approach, Universidade Católica Editora, Lisbona.
[4] Maurer R, Zilch K, Dunkelberg D, Kolodziejczyk A. Effektive Steifigkeiten, Anrechenbarkeit von Spanngliedern und heute unzulässige Bewehrungsformen beim Nachweis für Querkraft- und Torsion bei Bestandsbrücken. Bauing, Band 2014;89.
[5] Reichel, M. (2010) Dünnwandige Segmentfertigteilbauweisen im Brückenbau aus gefasertem Ultrahochleistungsbeton (UHFB) – Tragverhalten, Bemessung und Konstruktion. Dissertation, TU Graz.
[6] Shin, J. (2017) Ultra-High Performance Concrete (UHPC) Precast Segmental Bridges – Flexural Behaviour and Joint Design. Dissertation, TU Hamburg-Harburg. https://doi.org/10.15480/882.1370.
[7] Oettel V, Joachim L, Schmidt B. Calculation approach of multi keyed dry joints for sustainable modular precast element constructions made of UHPFRC. Constr Build Mater 2023;370(2023):130687. https://doi.org/10.1016/j.conbuildmat.2023.130687.
[8] Wilkening M, Schack T, Haist M, Oettel V. UHPFRC-Fertigteilsegmente für einen nachhaltigen und ressourcenschonenden Betonbrückenbau. Beton- und Stahlbetonbau 2023;118(No.11):788–802. https://doi.org/10.1002/best.202300054.
[9] Voo YL, Foster SJ, Voo CC. Ultrahigh-performance concrete segmental bridge technology: toward sustainable bridge construction. J Bridge Eng 2015;20. https://doi.org/10.1061/(ASCE)BE.1943-5592.0000704.
[10] Voo YL, Foster SJ. Characteristics of ultra-high performance 'ductile' concrete and its impact on sustainable construction. IES J Part A: Civ Struct Eng 2010;3:168–87. https://doi.org/10.1080/19373260.2010.492588.
[11] Oettel, V. (2016) Torsionstragverhalten von stahlfaserbewehrten Beton-, Stahlbeton- und Spannbetonbalken [Dissertation]. TU Braunschweig. https://doi.org/10.24355/dbbs.084–201606210916-0.
[12] Foster, S.J.; Voo, Y.L. (2015) UHPFRC as a Material for Bridge Construction: Are we making the most of our Opportunities? Conference Proceedings: CONCRETE 2015: Construction Innovation: Research Into Practice, Melbourne, Australia.
[13] Schmidt, M.; Fehling, E.; Geisenhanslüke, C. (2004) Ultra High Performance Concrete (UHPC) – Structural Materials and Engineering Series No. 3. International Symposium on Ultra High Performance Concrete 2004.
[14] Delauzun O, et al. Construction of the PS34 UHPFRC Bridge. Designing and Building with UHPFRC. John Wiley & Sons, London; 2011. p. 137–47. https://doi.org/10.1002/9781118557839.ch11.
[15] Vavel, A.: BFUP Béton d'exception pour innovations multiples – Pont de la Chabotte sur l'A51 (38). Construction Moderne – Annuel Overages d'Art 2005, Paris, pp. 30–32.
[16] Voo YL, Augustin PC, Thamboe TAJ. Construction and design of a 50 m single span UHP ductile concrete composite road bridge. Struct Eng 2011:24–31. No. 89, No. 15.
[17] Oettel V, Rieke A, Empelmann M. Production and testing of thin-walled UHPFRC precast elements. BFT Int 2014;80:64–74.
[18] Oettel V, Matz H, Empelmann M. Bestimmung der zentrischen Nachrisszugfestigkeit von UHPFRC mithilfe gekerbter 3-Punkt-Biegezugversuche. Beton- und Stahlbetonbau 2019;114:255–64. https://doi.org/10.1002/best.201800092.
[19] Grünberg J., Göhlmann J.. Concrete Structures for Wind Turbines. Berlin: Ernst & Sohn; 2013. https://doi.org/10.1002/9783433603291.
[20] Bögl S, Gläser C, Hierl M, Traute M. Vorgespannte Hybridtürme für Windenergieanlagen. Bauingenieur 2013;88:301–6.
[21] de Lana JA, et al. Behavior study of prestressed concrete wind-turbine tower in circular cross-section. 111403 Eng Struct 2021;22:1–15. https://doi.org/10.1016/j.engstruct.2020.111403.
[22] Huang X, Li B, Zhou X, Wang Y, Zhu R. Geometric optimisation analysis of steel-concrete hybrid wind turbine towers. Structures 2022;35:1125–37. https://doi.org/10.1016/j.istruc.2021.08.036.
[23] Klein F, Marx S. Effects of warping shear deformation on the torsional load-bearing behaviour of assembled half-shell structures for wind energy towers. 114728 Eng Struct 2022;269:1–15. https://doi.org/10.1016/j.engstruct.2022.114728.
[24] DIN 18088–2 (2019) Structures for wind turbines and platforms – Part 2: Concrete structures. Beuth, Berlin.
[25] Reichel, M.; Altersberger, G.; Sparowitz, L. (2011) UHPFRC Prototype for a Flexible Modular – Temporary High-speed Railway Bridge. Toutlemonde, F.; Resplendino, J. [Hrsg.] Designing and Building with UHPFRC – State of the Art and Development. London: ISTE Ltd / Hoboken: John Wiley & Sons, Inc.: pp. 263–277.
[26] EN 1991–2:2010–12 (2010) Eurocode 1: Actions on structures – Part 2: Traffic loads on bridges. European Committee for Standardization, Brussels.
[27] DIN EN 1991–2/NA:2012–08 (2012) German National Annex – Eurocode 1: Actions on structures – Part 2: Traffic loads on bridges. Beuth, Berlin.
[28] EN 1992–1-1:2011–01 (2011) Eurocode 2: Design of concrete structures – Part 1–1: General rules and rules for buildings. European Committee for Standardization, Brussels.

[29] DIN EN 1992–1-1/NA:2013–04 (2013) German National Annex – Design of concrete structures – Part 1–1: General rules and rules for buildings. Beuth, Berlin.
[30] Rossner, W.; Graubner, C.-A. (2012) Spannbetonbauwerke Teil 4: Bemessungsbeispiele nach Eurocode 2. Berlin: Ernst & Sohn.
[31] Deutscher Ausschuss für Stahlbeton (DAfStb) (2022) DAfStb-Richtlinie Ultrahochfester Beton – Teil 1: Bemessung und Konstruktion von Tragwerken aus stahlfaserbewehrtem ultrahochfesten Beton – Draft, Version 22.12.2022.
[32] ZTV-ING (2021) Zusätzliche Technische Vertragsbedingungen und Richtlinien für Ingenieurbauten. Bundesanstalt für Straßenwesen, 2021.
[33] SOFISTIK AG (2022) SOFISTIK Manual: ASE – General Static Analysis of FE Structures.
[34] Specker, A. (2001) Der Einfluss der Fugen auf die Querkraft- und Torsionstragfähigkeit extern vorgespannter Segmentbrücken [Dissertation]. TU Hamburg-Harburg. https://doi.org/10.15480/882.1060.
[35] Rettinger, M.; Lounis, A.; Hückler, A.; Schlaich, M. (2023) Druckversuche zur Ermittlung der Tragfähigkeit von ebenen und feinverzahnten Trockenfugen für modulare Segmentbrücken. Beton- und Stahlbetonbau. https://doi.org/10.1002/best.202300018.
[36] Oettel V, Empelmann M. Structural behavior of profiled dry joints between precast ultra-high performance fiber reinforced concrete elements. No. 1 Struct Concr 2019;20(2019):446–54. https://doi.org/10.1002/suco.201800117.
[37] Oettel V, Empelmann M. Feinprofilierte UHPFRC-Trockenfugen für Segmentbauteile. Beton- und Stahlbetonbau 2013;108(No. 7):487–95. https://doi.org/10.1002/best.201300024.
[38] Hughes TJR, Tezduyar TE. Finie elements based upon mindlin plate theory with particular reference to the four-node bilinear isoparametric element.. /3 J Appl Mech 1981;48:587–96. https://doi.org/10.1115/1.3157679.
[39] Tessler A, Hughes TJR. An improved treatment of transverse shear in the mindlin-type four quadrilateral element. Comput Methods Appl Mech Eng 1983;39:311–35. https://doi.org/10.1016/0045-7825(83)90096-8.
[40] Crisfield MA. A quadratic mindlin element using shear constraints. Comput Struct 1984;18:833–52. https://doi.org/10.1016/0045-7949(84)90030-0.
[41] Cañada Pérez-Sala J, Ruiz-Teran AM. Numerical analysis of precast concrete segmental bridge decks. Eng Struct 2023;275. https://doi.org/10.1016/j.engstruct.2022.115277.
[42] Turmo J, Ramos G, Aparicio AC. FEM modelling of unbonded post-tensioned segmental beams with dry joints. Eng Struct 2006;28:1852–63. https://doi.org/10.1016/j.engstruct.2006.03.028.
[43] Turmo J, Ramos G, Aparicio AC. FEM study on the structural behaviour of segmental concrete bridges with unbonded prestressing and dry joints: Simply supported bridges. Eng Struct 2005;27:1652–61. https://doi.org/10.1016/j.engstruct.2005.04.011.
[44] Yan W-T, et al. Research on numerical model for flexural behaviors analysis of precast concrete segmental box girders. Eng Stuct. 2020;219. https://doi.org/10.1016/j.engstruct.2020.110733.
[45] Yuan A, Dai H, Sun D, Cai J. Behaviors of segmental concrete box beams with internal tendons and external tendons under bending. Eng Struct 2013;48:623–34. https://doi.org/10.1016/j.engstruct.2012.09.005.
[46] Oettel V, Empelmann M. Druckstrebentragfähigkeit von vorgespannten UHPFRC-Hohlkästen unter Torsion und kombinierter Beanspruchung. No 3 Beton- und Stahlbetonbau 2014;109(2014):182–92. https://doi.org/10.1002/best.201300061.
[47] Rombach, G.A. (2002) Precast segmental box girder bridges with external prestressing - design and construction. Segmental Bridges. INSA Rennes. TU Hamburg-Harburg.
[48] Takebayashi T, Deeprasertwong K, Leung YW. A full-scale destructive test of a precast segmental box girder bridge with dry joints and external tendons. Struct Build – Proc Inst Civ Eng 1994;104(Issue 3):297–315. https://doi.org/10.1680/istbu.1994.26780.
[49] EN 1992–2:2010–12 (2010) Eurocode 2: Design of concrete structures – Part 2: Concrete Bridges – Design and detailing rules. European Committee for Standardization, Brussels.
[50] DIN EN 1992–2/NA:2013–04 (2013) German National Annex – Eurocode 2: Design of concrete structures – Part 2: Concrete Bridges – Design and detailing rules. Beuth, Berlin.
[51] DBV/BMV-Arbeitskreis „Bemessungsgrundsätze für Segmentbrücken“ (1999) Empfehlungen für Segmentfertigteilbrücken mit externen Spannngliedern. Bundesministerium für Verkehr, Bau- und Wohnungswesen.
[52] van der Horst, A.; Rombach, G.; Fischer, O. et al. (2017) Precast segmental bridges – Guide to good practice. Bulletin no. 82, Fédération Internationale du Béton (fib). Lausanne.
[53] Heek P, Look K, Oettel V, Mark P. Bemessung von Stahlfaserbeton und stahlfaserbewehrtem Stahlbeton. Beton- und Stahlbetonbau 116, Sonderh Stahlfaserbeton 2021:2–12. https://doi.org/10.1002/best.202100009.
[54] Bittner CM, Oettel V. Fiber reinforced concrete with natural plant fibers – investigations on the application of bamboo fibers in ultra-high performance concrete. Sustainability 2022;14(19):12011. https://doi.org/10.3390/su141912011.
[55] Ankay, B.; Metje, K.; Mönig, T.; Zhang, C.; Leutbecher, T. (2019) Ultrasonic characterisation of steel fibre orientation in ultra-high performance concrete. 20. GMA/ITG-Fachtagung Sensoren und Messysteme 2019.
[56] AFNOR - French standard institute (2016) National addition to Eurocode 2 – Design of concrete structures: specific rules for Ultra-High Performance Fibre-Reinforced Concrete (UHPFRC), Saint-Denis.
[57] Gleich, P.; Maurer, R. (2016) An analytical modelt o determine the shear capacity of prestressed continuous concrete beams. IABSE Congress: Challenges in Design and Construction of an Innovative and Sustainable Built Enviroment. Stockholm, Sweden. https://doi.org/10.2749/stockholm.2016.1539.
[58] Javidmehr S, Oettel V, Empelmann M. Schrägrissbildung von Stahlbetonbalken unter Querkraftbeanspruchung. Bauingenieur 2018;93. https://doi.org/10.37544/0005-6650-2018-06-58.
[59] Herbrand, M. (2017) Shear Strength Models for Reinforced and Prestressed Concrete Members. Dissertation. RWTH Aachen. https://doi.org/10.18154/RWTH-2017–06170.
[60] Herbrand, M.; Kueres, D.; Classen, M.; Hegger, J. (2018) Experimental Investigations on the Shear Capacity of Prestressed Concrete Beams with Rectangular and I-Shaped Cross-Sections. High-Tech Concrete: Where Technology and Engineering Meet. https://doi.org/10.1007/978–3-319–59471-2_78.
[61] Metje K, Leutbecher T. Verification of the shear resistance of UHPFRC beams – design method for the German DAfStb Guideline and database evaluation. Eng Struct 2023;277. https://doi.org/10.1016/j.engstruct.2022.115439.
[62] Busse, D.; Empelmann, M. (2015) Ultra-Light Concrete Members inspired by Bamboo. Stang, H.; Braestrup, M. [Hrsg.] Proceedings: Concrete – Innovation and Design. fib Symposium 2015, Copenhagen.
[63] Vestergaard, D.; Poulsen, P.N.; Hoang, L.C.; Larsen, K.P.; Feddersen, B. (2023) Design-oriented nonlinear-elastic buckling analysis of reinforced concrete wall structures using convex optimization. Structural Concrete. https://doi.org/10.1002/suco.202200883.
[64] Mark P, Oettel V, Look K, Empelmann M. Neuauflage DAfStb-Richtlinie Stahlfaserbeton. Beton- und Stahlbetonbau 2021;116(No. 1):19–25. https://doi.org/10.1002/best.202000065.
[65] Empelmann M, Oettel V, Cramer J. Berechnung der Rissbreite von mit Stahlfasern und Betonstahl bewehrten Betonbauteilen. Beton- und Stahlbetonbau 2020;115 (No. 2):136–45. https://doi.org/10.1002/best.201900065.
[66] Oettel, V.; Empelmann, M. (2015) Concrete Elements Reinforced with Large Diameters – Part 3: Columns. Proceedings of fib Symposium 2015, 18.–20.05.2015 in Kopenhagen (Denmark), pp. 114–115.
[67] Oettel V, Empelmann M. Große Stabdurchmesser und hohe Bewehrungsgrade – Teil 3: Druckglieder. Beton- und Stahlbetonbau 2018;113:789–98. https://doi.org/10.1002/best.201800061.
[68] Tankova T, Rodrigues F, Leitão C, Martins C, da Silva LS. Lateral-torsional buckling of high strength steel beams: experimental resistance. Thin-Walled Struct 2021;164. https://doi.org/10.1016/j.tws.2021.107913.
[69] Forman P, Penkert S, Kämper C, Stallmann T, Mark P, Schnell J. A survey of solar concrete shell collectors for parabolic troughs. Renew Sustain Energy Rev 2020;134:110331. https://doi.org/10.1016/j.rser.2020.110331.
[70] Forman P, Penkert S, Mark P, Schnell J. Design of modular concrete heliostats using symmetry reduction methods. Civ Eng Des 2020;2:92–103. https://doi.org/10.1002/cend.202000013.
[71] Grünberg, J.; Lohaus, L.; Ertel, C.; Elsmeier, K. (2014) Fatigue Behaviour of UHPC due to Uni- and Multiaxial Loading – Experimental Investigations and Development of a Mechanical Model. Sustainable Building with Ultra-High Performance Concrete, No. 22, Kassel university press GmbH, Kassel, 2014.
[72] Li L, Xu L, Huang L, Xu F, Huang Y, Cui K, et al. Compressive fatigue behaviors of ultra-high performance concrete containing coarse aggregate. Cem Concr Compos 2022;128:104425. https://doi.org/10.1016/j.cemconcomp.2022.104425.
[73] Tapsoba, N.; Citek, D.; Dobrusky, S.; Kolisko, J. (2017) Fatigue Behavior of Ultra-High Performance Concrete (UHPC) Under Compressive Loading. Proceedings of the AFGC-ACI-fib-RILEM Int. Symposium on Ultra-High Performance Fibre-Reinforced Concrete, pp. 291–300.
[74] Ye M, Li L, Yoo D-Y, Wang L, Li H, Shao X. Shear behaviour of precast ultrahigh-performance concrete (UHPC) segmental beams with external tendons and dry joints. Structures 2023;46:1696–708. https://doi.org/10.1007/s43452-023-00687-7.
[75] Liu T, Wang Z, Guo J, Wang J. Shear strength of dry joints in precast uhpc segmental bridges: experimental and theoretical research. 04018100 J Bridge Eng 2019;24(1):1–18. https://doi.org/10.1061/(ASCE)BE.1943-5592.0001323.
[76] Lanwer J-P, Oettel V, Empelmann M, Höper S, Kowalsky U, Dinkler D. Bond behavior of micro steel fibers embedded in ultra-high performance concrete subjected to monotonic and cyclic loading. Struct Concr 2019;20:1243–53. https://doi.org/10.1002/suco.201900030.
[77] Lanwer, J.-P.; Oettel, V.; Empelmann, M.; Höper, S.; Kowalsky, U.; Dinkler, D. (2019) Degradation Processes of UHPFRC under Cyclic Tensile Loading. Proceedings of the fib Symposium 2019: Concrete - Innovations in Materials, Design and Structures, pp. 1912–1919.
[78] Makita T, Brühwiler E. Tensile fatigue behavior of ultra-high performance fibre reinforced concrete (UHPFRC). Mater Struct 2014;47:475–91. https://doi.org/10.1617/s11527-013-0073-x.
[79] Oettel V, Lanwer J-P, Empelmann M. Auszugverhalten von Mikrostahlfasern aus UHPC unter monoton steigender und zyklischer Belastung. Bauingenieur 96 2021; Vol. 01-02:1–10.
[80] Fédération Internationale du Béton (2013) Model Code for Concrete Structures 2010. Ernst & Sohn.
[81] Speck, K.; Curbach, M. (2014) Experimental Determination and Mathematical Description of the Multiaxial Strength of Ultra-High Performance Concrete. Sustainable Building with Ultra-High Performance Concrete, No. 22, kassel university press GmbH, Kassel, 2014, pp. 365–392.